A prototype PET/SPET/X-rays scanner dedicated for whole body small animal studies

Maritina Rouchota[1] MSc,
Maria Georgiou[2] PhD,
Eleftherios Fysikopoulos[3] PhD,
Eirini Fragogeorgi[3,4] PhD,
Konstantinos Mikropoulos[3] MSc,
Panagiotis Papadimitroulas[2] PhD,
George C. Kagadis[1] PhD,
George Loudos[3,4] PhD

1.University of Patras, Rion, Patras, Greece
2.Bioemission Technology Solutions, Alexandras 116, Athens, Greece
3.Technological Educational Institute of Athens, Ag. Spiridonos 28, Egaleo, Athens, Greece
4.Institute of Nuclear & Radiological Sciences, Technology, Energy & Safety, NCSR "Demokritos", Greece

Keywords: Dedicated animal scanner -Molecular imaging, -Tri-modal system -SPECT/PET/CT

Corresponding author:
Maritina Rouchota, MSc
University of Patras, Rion,
Patras, Greece
0030 694 2701625
m.rouchota@upatras.gr

Received:
5 May 2017
Accepted revised:
10 July 2017

Abstract

Objectives: To present a prototype tri-modal imaging system, consisting of a single photon emission computed tomography (SPET), a positron emission tomography (PET), and a computed tomography (CT) subsystem, evaluated in planar mode. **Materials and Methods:** The subsystems are mounted on a rotating gantry, so as to be able to allow tomographic imaging in the future. The system, designed and constructed by our group, allows whole body mouse imaging of competent performance and is currently, to the best of our knowledge, unequaled in a national and regional level. The SPET camera is based on two Position Sensitive PhotoMultiplier Tubes (PSPMT), coupled to a pixilated Sodium Iodide activated with Thallium (NaI(Tl)) scintillator, having an active area of 5x10cm^2. The dual head PET camera is also based on two pairs of PSPMT, coupled to pixelated berillium germanium oxide (BGO) scintillators, having an active area of 5×10cm^2. The X-rays system consists of a micro focus X-rays tube and a complementary metal-oxide-semiconductor (CMOS) detector, having an active area of 12x12cm^2. **Results:** The scintigraphic mode has a spatial resolution of 1.88mm Full Width at Half Maximum (FWHM) and a sensitivity of 48cps/MBq at the collimator surface. The coincidence PET mode has an average spatial resolution of 3.5mm and a peak sensitivity of 13483cps/MBq. The X-rays spatial resolution is 3.5lp/mm and the contrast discrimination function value is lower than 2%. **Conclusion:** a compact tri-modal system was successfully built and evaluated for planar mode operation. The system has an efficient performance, allowing accurate and informative anatomical and functional imaging, as well as semi-quantitative results. Compared to other available systems, it provides a moderate but comparable performance, at a fraction of the cost and complexity. It is fully open, scalable. and its main purpose is to support groups on a national and regional level and provide an open technological platform to study different detector components and acquisition strategies.

Hell J Nucl Med 2017; 20(2): 146-153 *Epub ahead of print: 12 July 2017* *Published online: 8 August 2017*

Introduction

Small animal imaging has been the driving force in preclinical research, as well as for the development of imaging technology over the last two decades [1]. In high performance positron emission tomography (PET) and single photon emission tomography (SPET), position sensitive photomultiplier tubes (PSPMT) have offered clear advantages regarding the energy estimation and positioning of gamma ray interactions allowing the construction of robust and compact systems, suitable for mouse imaging [2, 3]. High resolution functional images produced by such dedicated nuclear medicine systems can be fused with high resolution anatomical images, producing a thorough detailed image of biodistribution and pharmacokinetics, with precise localization properties [4, 5].

Such dedicated multimodal imaging systems are commercially available, but their high purchase and maintenance costs make them unapproachable to the majority of research groups. Considering that many small and medium teams work in the development of new radiopharmaceuticals and evaluate new biomolecules (including nanoparticles) or study disease models [6-8], the development of low cost systems, with sufficient performance addresses existing needs. By selecting the proper detector components and acquisition strategies, it is possible to achieve a good compromise between performance and cost.

In this work, we have designed a tri-modal system combining three basic imaging modalities (SPET/PET/CT) (Figure 1). The main purpose of the system is to support groups on a national and regional level. Moreover, it provides an open technological platform to study different detector components and acquisition strategies, including scintillators and collimators for imaging higher energy isotopes. It has been evaluated in planar mode

using technetium-99m (^{99m}Tc) for scintigraphic imaging and gallium-68 (^{68}Ga) for coincidence imaging, while tomographic mode and studies with other low energy isotopes are possible.

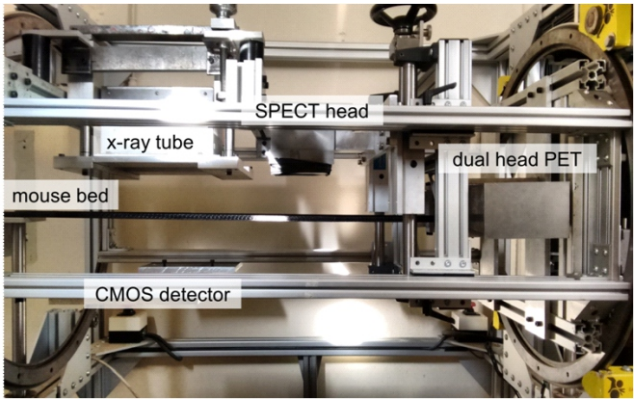

Figure 1. Image of the constructed tri-modal small animal imaging system.

Materials and Methods

SPET subsystem

The SPET camera is based on two square H8500 flat-panel PSPMTs (Hamamatsu, Japan) in a 1×2 arrangement and total dimensions 105.7×52×34mm^3. The two PSPMTs are coupled to a pixelated sodium iodide activated with thallium (NaI(Tl)) crystal (SaintGobain, France) with an active area of 97.4×44.8mm^2. The pixel dimensions are 1×1×5mm^3 with a pitch of 1.2mm. The array is viewed through a 3mm glass window and encapsulation is completed by an aluminum cover, 50μm thick. Optical grease BC-630 (SaintGobain, France) has been used for optical coupling of the PSPMTs to the scintillation layer. A general purpose parallel-hole lead collimator is used (Nuclear Fields Co, Netherlands), with hexagonal holes of 1.2mm inner diameter and 0.2mm thick septum walls. Its height is 25mm, with an active area of 52×105 mm^2. The system is enclosed in an 8mm tungsten (W) housing box of 140×82×107mm^3.

Initially, data were acquired using two PCI cards, a G3 Mac and Kmax software by Sparrow Corporation [9]. To decrease the size, cost and flexibility, a new readout was implemented. Camera output analog signals were digitized at 50MHz sampling rate using 12-bit resolution free running analog to digital converters (ADC) (Texas Instruments ADS5282). An embedded system based on MicroBlaze microprocessor (Xilinx Inc, US) was developed at a Spartan 6 LX150T FPGA development board (Avnet Inc, US) for data acquisition and processing of the digitized signals. The data acquisition method is described in detail in [10]. For the new acquisition architecture the optimal HV was found to be equal to - 865V for technetium-99m (^{99m}Tc) imaging.

The system is accompanied by a user-friendly interface that supports acquisition, data base for raw data and image archiving, DICOM (Digital Imaging and Communications in Medicine) format, basic data processing tools, and reporting, so that images and corresponding analyses are exported in PDF format.

PET subsystem

Each head of the developed dual head PET system is also based on a pair of two square H8500 flat-panel PSPMTs. The PSPMTs are coupled to a 5×10cm^2 bismuth germanium oxide (BGO) scintillator array (Hilger Crystals Ltd, UK), with a pixel size of 2×2×5mm^3 and 0.25mm septa. Each head is enclosed in a 5 mm tungsten (W) housing box of approximately 135×135×80mm^3 and mounted on the rotating gantry, placed one physically opposed to the other, at an 80mm distance. Currently, the system works in coincidence mode, where only crystals with a certain angle (acceptance angle) are allowed to contribute coincidences. This effect has been studied by our group [11], where it has been shown that as the acceptance angle decreases, the spatial resolution and the uniformity of the field of view (FOV) increase, but the sensitivity decreases as well. The final image is a projection in a plane, which is located at the middle of the two heads. In this implementation, the acceptance angle is 10 degrees, which offers a good compromise between sensitivity and resolution, while the FOV is 5×10cm^2 to allow whole body mouse imaging. Predefined acquisition parameters are a timing window of 16ns and an energy window between 350-700keV. Digitization was performed with the aforementioned ADC present in the SPET system, using a sampling frequency of 65MHz. The Spartan 6 LX150T development board was used again for the acquisition and processing of the acquired signals. The data acquisition method is described in detail in [12].

X-rays subsystem

The developed X-rays system consists of an X-rays tube and a CMOS detector, mounted on the rotating gantry and separated by a distance of 30cm, to allow whole body imaging in a single shot. The X-ray tube used is a Source-Ray Inc. SB-80-500-DI (Source-Ray Inc), operated between 35kVp and 80 kVp with a tube current up to 0.5mA. The tube has a fixed W anode, tilted by 20 degrees with respect to the electron beam axis, a 0.8mm carbon fiber exit window, a 33μm minimum focal spot size and an inherent filtration of 1.8mm Al at 80kVp.

The CMOS Flat Panel Sensor used is the C10900D model by Hamamatsu. It is a high resolution sensor with a CsI scintillator layer directly deposited on a 2D photodiode array. The minimum pixel size is equal to 0.1mm and the active area is approximately 12×12cm^2 (1216×1232 pixels in the 'fine' scan mode). It supports incident beam energies up to 90 kVp, so it is in good accord with the chosen X-rays tube.

System evaluation

The scintigraphic performance evaluation was based on previously published literature on small field-of-view gamma cameras performance [13, 14]. The coincidence performance evaluation was also based on previously published literature, on benchtop PET preclinical systems [15, 16]. The coincidence images were reconstructed through the Focal

Plane Tomography (FTP) algorithm, which is used by many groups for the evaluation of dual PET planar detectors [17, 18]. The evaluation of the X-ray system was based on the AAPM TG-74 report [19].

SPET evaluation

Uniformity

The intrinsic uniformity of the detector was calculated by removing the collimator and placing a ^{99m}Tc point source of 3.7 MBq at a distance of 5 times the UFOV. A total of 7×106 counts were collected. For the system uniformity the collimator was kept in place and a ^{99m}Tc flood source of 18.5MBq was placed upon the collimator. A total of 8.5×106 counts were collected.

Both images were then processed with a [1 2 1; 2 4 2; 1 2 1] weighted filter. The integral uniformity was calculated as the coefficient of deviation, i.e. the standard deviation of counts divided by the mean number of counts in the image. The differential uniformity was calculated as the difference between the maximum and minimum count of the region divided by their sum, for any 5 consecutive pixels in all rows and columns [13]. For the system uniformity both the useful field of view (UFOV, i.e. the field seen by the collimator holes) and for the central field of view (CFOV, i.e. the 75% central region of the UFOV) were studied.

Count rate capability

The system's count rate capability was evaluated using 3 cylindrical phantoms 40mm long and 5mm in diameter filled with different activities of ^{99m}Tc. The sources were measured prior to the experiment in a Geiger tube counter, to calculate the actual ratio between the activities. The values extracted from the counter were 2.405MBq (1), 7.77MBq (2), and 25.9MBq (3), corresponding to actual ratios of 10.8 (3:1), 3.3 (3:2) and 3.2 (2:1). These ratios were then measured on the acquired image and the results were compared to determine and quantify deviations.

Energy resolution

The energy spectra were obtained using a ^{99m}Tc source (~0.37 MBq) placed at 1m distance from the surface of the scintillator, after removing the collimator. For each crystal pixel, the energy spectrum was acquired and an automated algorithm was used to find and record the photopeak channel in all pixels. All spectra were normalized to the same photopeak position by multiplying each value of the spectrum with the ratio of the selected normalized photopeak (at 140 keV) with the current photopeak. The normalized energy spectrum is the sum of all individual spectra of the crystal elements, after applying these corrections for each pixel of the array. A Gaussian fit was applied to the normalized energy spectrum and the energy resolution was determined for 140keV energy peak, using the standard Full Width at Half Maximum (FWHM).

Spatial resolution

To evaluate the spatial resolution of the scintigraphic system a capillary filled with a ^{99m}Tc solution was used. The capillary having an inner diameter of 1.1mm and a length of 90mm was placed with a slight inclination (3 pixels wide from top to bottom) at different distances from the collimator. Spatial resolution was calculated as the FWHM of the line spread function (LSF) from the line profile of the capillary source at three different points along the capillary length, for each distance. The average value and standard deviation for each distance was used. To verify the measured spatial resolution, a simple test was also performed, by placing two capillaries at a distance of 2mm in the center of the field of view. The image and the corresponding profiles were drawn.

Sensitivity

Sensitivity was measured using data of the previous experiment, by placing the capillary source at the center of FOV, at different distances from the collimator. System sensitivity was defined as the recorded counts in the flood corrected image, within a ±20% energy window around the 140keV photopeak, per second divided by the decay-corrected activity of the source in Mbq.

PET evaluation

Energy resolution

The energy resolution was measured following the same procedure as for the scintigraphy evaluation, but with a ^{68}Ga flood source placed in the middle of the head-to-head distance, which is 80mm. We have selected ^{68}Ga as a PET source, since our group has access to a Gallium generator.

Spatial resolution

The spatial resolution of the system, in coincidence mode, was evaluated by using a capillary, with an inner diameter of 1.1mm and length of 65mm, filled with ^{68}Ga solution. The capillary source was moved linearly across the horizontal and vertical direction, in the mean plane among the two opposite parallel detectors, while taking coincidence count rate profiles on reconstructed coincidence images. The average value of the measured FWHM was used for each direction. To verify the measured spatial resolution, a simple test was also performed, by placing two capillaries at a distance of 4mm in the center of the field of view. The image and the corresponding profile were extracted.

Sensitivity

Sensitivity was measured with a 0.037MBq ^{22}Na point source, placed in the middle of the head-to-head distance. Three positions were considered, one at the center of the field of view and two near the edges. System sensitivity was determined as the recorded coincidence counts, within the 350-700keV energy window, per minute, divided by the decay-corrected activity of the source. The coincidence timing window was set equal to 16ns.

X-rays Evaluation

Beam quality

For the assessment of the beam quality of the X-ray beam the RaySafe Xi dosimeter (RaySafe) with the R/F (Radiography/Fluroscopy) Classic external detector was used. The low

dose rate mode was chosen, suitable for measuring dose rates of <1mGy/sec. The dose rate at the detector surface was monitored, by placing an increasing thickness of aluminum filter (0.5 to 5mm) at the tube exit window. The aluminum thickness for which the initial dose rate is reduced to half (half value layer) was estimated for 3 main operating tube voltages.

Spatial resolution

For the evaluation of the spatial resolution of the X-ray system the TOR ^{18}FG imaging performance test object (Leeds Test Objects Ltd) was used. Its inner central region incorporates appropriate bar pattern structures ranging between 0.5 to 5lp/mm. The test object was imaged by choosing 35kVp, 500μA and 0.1s exposure time.

Low contrast sensitivity

For the low contrast sensitivity assessment, the same test object was used, as it incorporates appropriate structures for different contrast induction on its periphery. The test object was imaged with 70kVp and an additional filter of 1mm Cu, as proposed by the manufacturer (Leeds Test Objects Ltd).

Animal Studies

Three mice purchased from the breeding facilities of the National Center for Scientific Research "Demokritos", Athens, Greece, were used for a proof of concept imaging study and were kept under environmentally controlled conditions, in individually ventilated cages, with food and water ad libitum.

Anesthetization was performed intra-peritoneally (i.p.) with 100μL/10g body weight of a stock solution containing 10% ketamine–hydrochloride (100mg/mL), 5% xylazine-hydrochloride (20mg/mL) prior to scanning. The imaging studies were then performed as described below.

a) All three mice were imaged in the X-ray system just before the radioisotope administration, to maintain the exact same positioning and to be used for image fusion. The imaging parameters were set to 35kVp, 500μA and 0.1s exposure time.

b) Two female normal Swiss-Webster Albino mice (32 and 20g, respectively) were used for the scintigraphic imaging study. 100μL of approximately 21.2MBq of technetium medronic acid (^{99m}Tc-MDP) were administered to the first mouse, through the tail-vein, subsequent to anaesthesia. The same procedure was followed with the second mouse, by administering 7.4MBq of technetium hexamethylpropyleneamineoxime (^{99m}Tc-HMPAO). Then, the mice were placed on the animal bed at a <0.5 cm distance from the camera head to allow imaging with maximum spatial resolution and successive 2min frames were collected for up to 1h post injection (p.i.). All frames were summed, to achieve an image with high statistics, while processing on each frame is possible.

3) A male SCID mouse (23g), administered with 4T1 cancer cells, was used for the coincidence imaging study. ^{68}Ga labelled iron oxide nanoparticles (NP) were administered through the tail vein and passive targeting on tumor was expected. The administered activity was 5.18 MBq of ^{68}Ga. Successive 2min frames were collected for up to 3h p.i. Frames were summed, to achieve images with higher statistics.

Results

Performance indices

Evaluation of SPET performance

Uniformity

The intrinsic and system uniformity are reported in Table 1. For the system uniformity both the UFOV and CFOV are studied. The uniformity values obtained for our system are in good accord with studies on similar imaging systems [20].

Table1. *The uniformity values obtained for the scintigraphy system.*

	Intrinsic uniformity	System uniformity	
	Full field	UFOV	CFOV
Coefficient of variation (%)	9.2	9.3	8.2
Differential uniformity (%)	5..3	5.6	4.5

Count rate capability

The 3 cylinders filled with different activities of ^{99m}Tc are seen in Figure 2. The measured activity ratios were 10.2 (3:1), 3.2 (3:2) and 3.2 (2:1) respectively, yielding a maximum deviation of 5% from the actual ratio values measured in the Geiger tube, proving a good overall count rate capability of the scintigraphic system. No distortions are observed at the middle of the image, where the two PSPMT are glued together, creating a dead area below the scintillator.

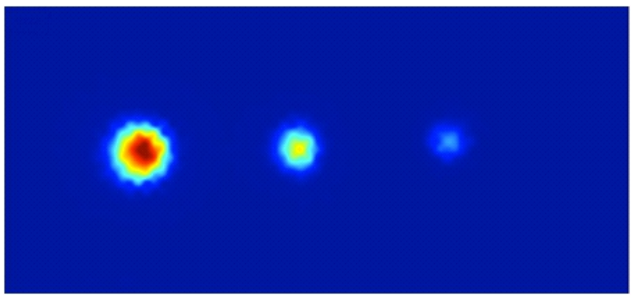

Figure 2. Three cylinders of different activities to estimate the count rate capability of the scintigraphic field of view. A maximum deviation of 5% from nominal values is observed, yielding a good system count rate capability.

Energy resolution

The energy resolution measured through the normalized spectrum over all crystals is 19.2%. This value is considered adequate for small animal imaging studies, where the scatter contribution is relatively small. The difference com-

pared to standard continuous scintillators is mainly attributed to the small pixels of the crystal, which result to multiple light reflections inside each pixel.

Spatial resolution

The measured spatial resolution for scintigraphic imaging, when in contact with the collimator, is 1.88±0.2mm. At the 10-20mm distance, where the mouse organs are usually located, the resolution rises to ~3mm. The spatial resolution curve is shown in Figure 3.

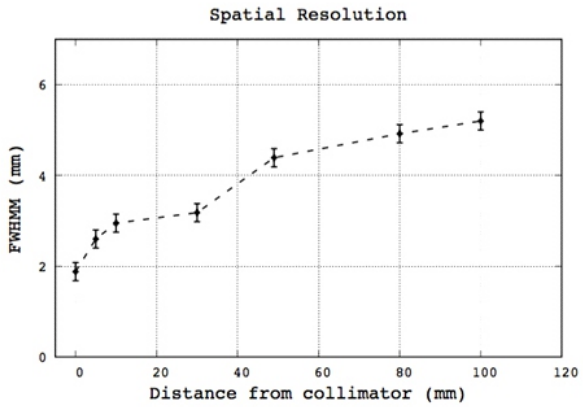

Figure 3. The spatial resolution of the scintigraphic system as a function of source-to-collimator distance. A minimum value of 1.88mm is observed at the collimator surface.

To verify the measured spatial resolution, a simple test was performed, by placing two capillaries at a distance of 2mm. The image and the corresponding profile are shown in Figure 4. It can be seen that the two capillaries are clearly distinguished, as expected from the calculated spatial resolution of 1.88mm.

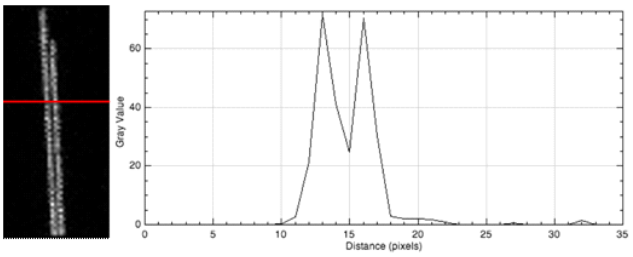

Figure 4. Two capillaries separated by a distance of 2mm and the corresponding profile.

Sensitivity

The measured sensitivityfor the scintigraphic system is 48± 1cps/MBq for a ±20% energy window. The values of the sensitivity with respect to the source-to-collimator distance can be seen in Figure 5. As expected for parallel-hole collimation [21], a decrease is observed when distance is increased.

Evaluation of PET performance

Energy resolution

The energy resolution, measured through the averaged spectrum over all crystals for the coincidence imaging, is 30%, which is in agreement with other similar systems that use BGO scintillators [22]. It must be noted that variations in the energy response have also been observed by using the same material, but from different providers.

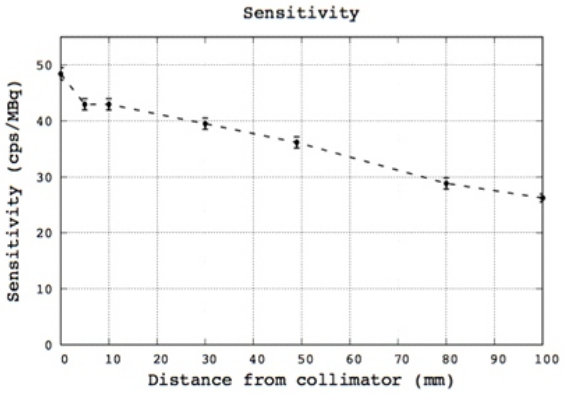

Figure 5. The sensitivity of the scintigraphic system, as a function of source-to-collimator distance. A maximum value of 48±1cps/MBq is observed at the collimator surface. The energy window was ±20%.

Spatial resolution

The spatial resolution for the x plane is measured to be 3.73± 0.17mm and for the x plane 3.27±0.03mm. Taking into account the relatively high positron range of ^{68}Ga, it is likely that the actual spatial resolution is even better. To verify the spatial resolution, a simple test was also performed, by placing two capillaries at a distance of 4mm. The capillaries can be clearly separated as it is shown by the image and the corresponding profile in Figure 6.

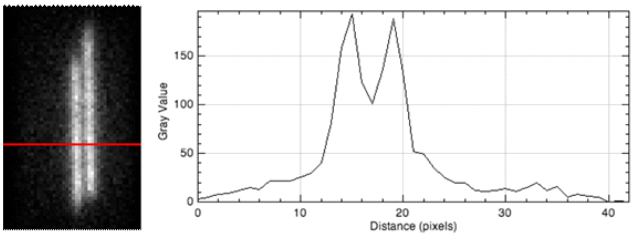

Figure 6. Two capillaries separated by a distance of 4mm and the corresponding profile.

Sensitivity

The sensitivity for the coincidence imaging is measured equal to 13483cps/MBq for a 350-700keV energy window. The sensitivity with respect to source positioning is shown in Figure 7.

Evaluation of X-rays performance

Beam quality

The estimation of the beam quality that was performed through measuring the HVL in mm of Al for 3 different tube voltages, is presented in Figure 8. The HVL values extracted

are 1.22mm, 1.48mm and 2.06mm of Al for tube voltages of 35kVp, 50kVp and 80kVp respectively.

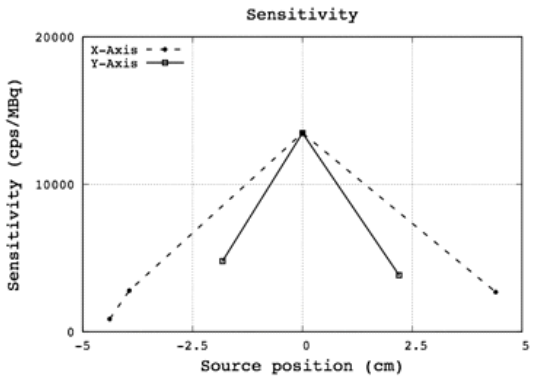

Figure 7. Sensitivity of the coincidence system for the two axes, at the centre and at the edges of the field of view. A maximum value of 13483cps/MBq is observed at the center of the field. The energy window was 350-700keV.

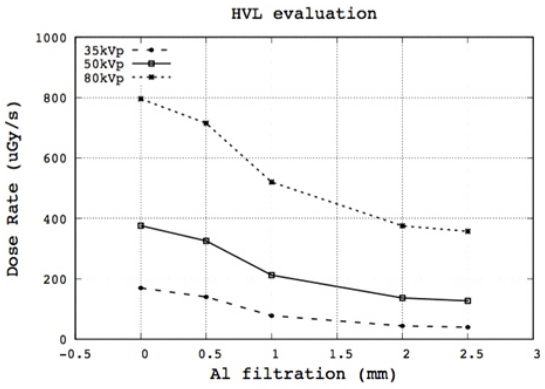

Figure 8. HVL estimation, in mm of Al filtration, of the x-ray beam for 3 operating voltages. HVL of 1.22mm, 1.48mm and 2.06mm for 35kVp, 50kVp and 80kVp respectively are measured.

Spatial resolution

The results for the spatial resolution can be seen in Figure 9. It is estimated to be 3.5lp/mm, which is in accord with the detector's specifications, for the fine and panoramic operation mode. This value is sufficient for performing studies in mice, especially if the role of X-rays imaging is to provide an anatomical map for the radioisotopic studies.

Low contrast sensitivity

The low contrast sensitivity evaluation is shown in Figure 10. As the test object exceeded the dimensions of the detector, two consecutive acquisitions were performed, one for the upper and one for the lower part of the test object. Structures of < 2% contrast induction can be distinguished.

Animal Studies

X-rays imaging

An X-ray image was acquired prior to the scintigraphic and coincidence acquisitions, both for fusion purposes and for evaluating the X-rays system performance (Figure 11). It can be seen that even very slight details and small structures can be easily distinguished.

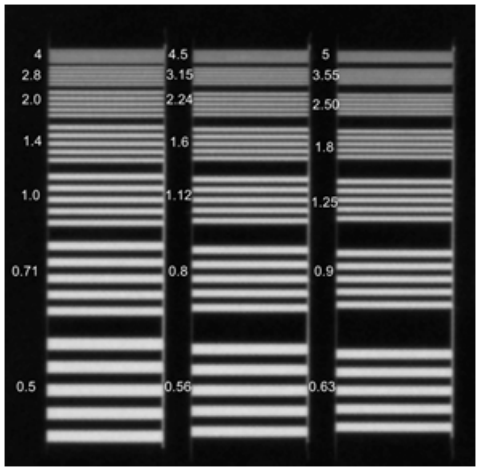

Figure 9. Spatial resolution estimation for the X-rays system. The bar pattern of 3.55lp/mm can be easily distinguished.

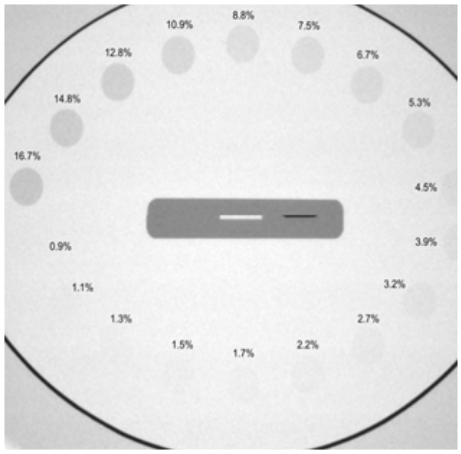

Figure 10. Low contrast sensitivity evaluation for the X-rays system. The structure inducing a contrast of 2% can be easily distinguished.

Scintigraphic imaging

The scintigraphic images acquired as described in 2.4.4 are shown in Figures 12 and 13, together with the fused images.

The expected normal distributions of both ^{99m}Tc-MDP and ^{99m}Tc-HMPAO are observed, with high concentration in the bones or in the brain, many internal organs and the bladder. The fusion with the X-rays image facilitates the determination of hot spots location in the mouse body, especially in a tracer with localization in various and different organs. Apart from the visual assistance, the X-rays information can be also used for drawing regions of interest on selected organs or structures.

Coincidence imaging

The coincidence image acquired as described in 2.4.4 is shown in Figure 14, along with the fusion image. As it is expected for non-targeted iron oxide nanoparticles, high concentration in liver and a noticeable accumulation on the

tumor region (left shoulder) due to the enhanced permeability and retention (EPR) effect are observed. Again, the X-rays image supports the accurate location of PET findings.

Figure 11. An X-rays acquisition of 35kVp, 0.5mA and an exposure time of 0.1s.

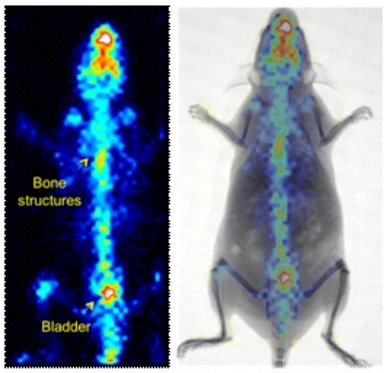

Figure 12. A scintigraphic acquisition of 1h with ^{99m}Tc-MDP and the fusion image with the mouse X-rays.

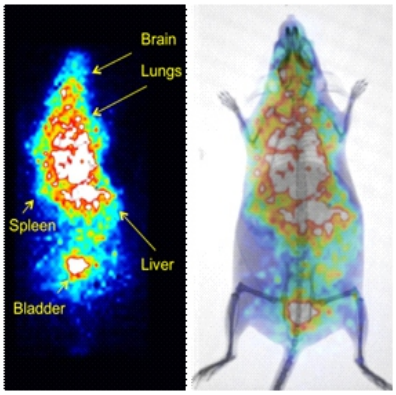

Figure 13. A scintigraphic acquisition of 1h with ^{99m}Tc-HMPAO and the fusion image with the mouse X-rays.

Discussion

A custom trimodal SPET/PET/CT system has been designed and evaluated, in planar mode. To the best of our knowledge, there is currently no other custom SPET/PET/CT system with published results that provides the combination of the three imaging modalities, together with the possibility of tomographic imaging.

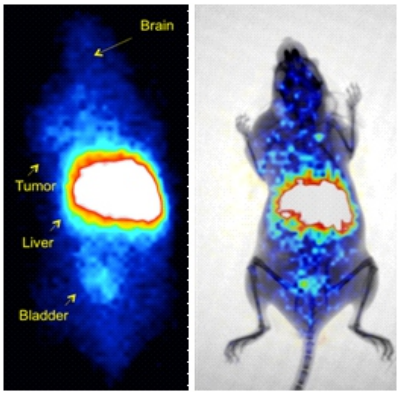

Figure 14. Coincidence acquisition of 3hrs duration with ^{68}Ga labelled on iron oxide NPs and the fusion image with the mouse X-rays.

The system offers a spatial resolution of 1.8mm in scintigraphic imaging and 3.5mm in coincidence mode. The field of view in both modalities allows for whole body mouse imaging. While many high-performance systems offer a spatial resolution in the order of 1mm [4, 5, 14, 21], it should be taken into account that such systems are usually based on multipinhole collimators and require tomographic mode that does not allow fast dynamic studies. In addition, they do not always permit whole body acquisitions or they use minification, which decreases their resolution for whole body imaging too. Finally, they all have limitations in terms of cost and complexity, as mentioned above. For the planar PET resolution, again there are systems providing spatial resolution in the order of 2mm [4, 5, 11, 15], but are also based on far more expensive components. However, our spatial resolution is considered adequate for planar PET screening studies, as in the case of scintigraphic imaging. By optimizing the processing of coincidences in both heads, further improvement is possible and the expected resolution limit is the crystal's pixel size. For the majority of initial screening studies, information on the in vivo behavior of a new tracer is the first evaluation step. Thus, fast, whole body information is required and in this case a resolution in the order of 2 to 3mm can provide sufficient information to screen various products and select which should be further studied.

The scintigraphic sensitivity of the system allows for dynamic studies to be performed both for scintigraphic and coincidence mode. From our experience, even short scans of 10 secs provide accurate information for drawing time activity curves at the first minutes post injection. Depending on the application, sensitivity can be further improved by alternative collimator selection. Taking into account that in a planar study the organs are located at a depth of 1-2cm, it is possible to investigate other collimator designs i.e. square collimator that significantly increase sensitivity while maintaining resolution at small distances. On the other hand, the coincidence sensitivity is higher by almost two orders of magnitude, compared to the scintigraphic component, demonstrating the added value of PET and being in good agreement with literature [1, 4]. Further improvement in sen-

sitivity is expected if the coincidence data from both heads are processed by using all possible coincidence angles, which is considered as a next step in our work.

The x-ray system's spatial resolution is estimated to be 3.5 lp/mm, which is in accord with the detector's specifications, for the fine and panoramic operation mode. This value is sufficient for performing studies on mice, especially if the role of x-ray imaging is to provide an anatomical map for the radioisotopic studies. It is within our intention to further explore the limits of X-rays imaging, by including dual energy imaging, in order to enhance specific structures and/or test longer exposure times. The system offers also the possibility to focus on particular parts of the animal and improve resolution if required.

The imaging studies that have been performed also clearly demonstrate that the system can be efficiently used for the evaluation of a novel agent, with good resolution and sensitivity for SPET and PET tracers. In addition, the benefits of fusing this information with anatomic data from X-ray are obvious, especially when testing new tracers with unknown biodistribution.

In conclusion, the presented system is fully open, scalable. and its main purpose is to support groups on a national and regional level. It also provides an open technological platform to study different detector components and acquisi--tion strategies, including scintillators and collimators for imaging higher energy isotopes. Current work includes the evaluation in tomographic mode, as well as extension to allow imaging of higher energy therapeutic isotopes. Future work includes the addition of two more heads for the PET component and a second SPET head to improve overall sensitivity.

All applicable international, national, and/or institutional guidelines for the care and use of animals were followed.

Acknowledgements

The authors would like to thank Dr. Penelope Bouziotis, head of the Radiochemical Studies Laboratory, NCSR "Demokritos" for providing the ^{68}Ga labelled nanoparticles for PET imaging. This work was supported by the Research Projects for Excellence IKY/Siemens, the European Union (European Social Fund) and Greek national resources under the framework of the "ARISTEIA II" project HYPERGNOSTIC code 4309 of the "Education & Lifelong Learning" Operational Programme and by the H2020-MSC-RISE project VIVOIMAG (645757).

The authors of this study declare no conflict of interest

Bibliography

1. Kagadis G. C., Loudos G., Katsanos K. et al. In vivo small animal imaging: current status and future prospects. *Medical Physics* 2010, 37(12), 6421-42,
2. Pani R., R. Scafe, R. Pellegrini et al. Scintillation arrays characterization for photon emission imaging. *Nuclear Instruments and Methods in Physics* Research Section A: Accelerators, Spectrometers, Detectors and Associated Equipment 2002; 477, no. 1: 72-6.
3. Pani R., A. Pergola, R. Pellegrini et al. New generation position-sensitive PMT for nuclear medicine imaging. Nuclear In*struments and Methods in Physics* Research Section A: Accelerators, Spectrometers, Detectors and Associated Equipment, 1997; 392, no. 1-3: 319-23.
4. Sánchez F., A. Orero, A. Soriano et al. ALBIRA: a small animal PET/SPECT/CT imaging system. *Medical physics* 2013; 40, no.5.
5. Magota Keiichi, Naoki Kubo, Yuji Kuge et al. Performance characterization of the Inveon preclinical small-animal PET/SPECT/CT system for multimodality imaging. *European journal of nuclear medicine and molecular imaging* 2011; 38, no. 4: 742-52.
6. Toyama, Hiroshi, Daniel Ye, Masanori Ichise et al. PET imaging of brain with the β-amyloid probe, [^{11}C] 6-OH-BTA-1, in a transgenic mouse model of Alzheimer's disease. *Eur J Nucl Med and Mol Im* 2005; 32, no. 5: 593-600.
7. Casteels C, P. Vermaelen, J. Nuyts et al. Construction and evaluation of multitracer small-animal PET probabilistic atlases for voxel-based functional mapping of the rat brain. *J Nucl Med* 2006; 47, no. 11: 1858-66.
8. Lewis J. S., S. Achilefu, J. R. Garbow et al. Small animal imaging: current technology and perspectives for oncological imaging. *Eur J of Cancer* 2002; 38, no. 16: 2173-88.
9. Loudos G., S. Majewski, R. Wojcik et al. Performance Evaluation of a Dedicated Camera Suitable for Dynamic Radiopharmaceuticals Evaluation in Small Animals, *IEEE Trans. Nucl. Sc*, Vol. 54, No. 3, June 2007.
10. Fysikopoulos E., G. Loudos, M. Georgiou et al. A Spartan 6 FPGA-based data acquisition system for dedicated imagers in nuclear medicine, *Measurement Science and Technology* 2012; Vol. 23, No. 12.
11. Efthimiou N., S. Maistros, X. Tripolitis et al. Tomographic evaluation of a dual head PET, *Meas Sci Technol* 2011, 22, 114010 (10pp).
12. Fysikopoulos E., M. Georgiou, N. Efthimiou et al. Fully Digital FPGA-Based Data Acquisition System for Dual Head PET Detectors, *IEEE Transactions on Nuclear Science* 2014; Vol. 61, No. 5.
13. Bhatia B.S., S. L. Bugby, J. E. Lees, and A. C. Perkins, A scheme for assessing the performance characteristics of small field-of-view gamma cameras, *Phys. Medica* PM Int. J. Devoted Appl. Phys. Med. Biol. Off. J. Ital. Assoc. Biomed. Phys. AIFB , Feb. 2015, vol. 31.
14. Bugby S. L., J. E. Lees, B. S. Bhatia, and A. C. Perkins, Characterisation of a high resolution small field of view portable gamma camera, P*hys Medica* PM Int. J. Devoted Appl. Phys. Med. Biol. Off. J. Ital. Assoc. Biomed. Phys. AIFB, May 2014; Vol. 30, no. 3.
15. Zhang H., Q. Bao, N. T. Vu et al. Performance Evaluation of PETbox: A Low Cost Bench Top Preclinical PET Scanner, *Mol Imaging Biol*, Oct. 2011; Vol. 13, no. 5, pp. 949–61.
16. Alva-Sánchez H., A. Martínez-Dávalos, E. Moreno-Barbosa et al. Initial characterization of a benchtop microPET system based on LYSO crystal arrays and Hamamatsu H8500 PS-PMTs. *Nuclear Instruments and Methods in Physics Research* Section A: Accelerators, Spectrometers, Detectors and Associated Equipment 604, 2009, no. 1: 335-8.
17. Zhang J., Olcott, P. D., Chinn, G. et al. Study of the performance of a novel 1mm resolution dual-panel PET camera design dedicated to breast cancer imaging using Monte Carlo simulation. *Med Phys* 2007; 34: 689–702.
18. Smith M. F., R. R. Raylman, S. Majewski, and A. G. Weisenberger, Positron emission mammography with tomographic acquisition using dual planar detectors: initial evaluations, *Phys Med Biol*, Jun. 2004; Vol. 49, no. 11, p. 2437.
19. Shepard S. J., Pei-Jan Paul Lin, and J. M. Boone. Quality control in diagnostic radiology, 2002, *AAPM:* Report 74.
20. Stolin A. V., M. B. Williams, B. K. Kundu et al. Characterization of imaging gamma detectors for use in small animal SPECT. *In Nuclear Science Symposium Conference Record* 2003 *IEEE,* vol. 3, pp. 2085-9. IEEE.
21. Moji V., Zeratkar N, Farahani MH et al. Performance evaluation of a newly developed high-resolution, dual-head animal SPECT system based on the NEMA NU1-2007 standard, *J Appl Clin Med Phys* 2014, 15(6): 49-36.
22. Zhang H., N. T. Vu, Q. Bao et al. Performance characteristics of BGO detectors for a low cost preclinical PET scanner. *IEEE transactions on nuclear science* 57 2010, no. 3: 1038-44.